Synthesis of a Li−Mn-oxide with Disordered Layer Stacking through Flocculation of Exfoliated MnO_2 Nanosheets, and Its Electrochemical Properties

Lianzhou Wang, Kazunori Takada,† Akihisa Kajiyama, Mitsuko Onoda, Yuichi Michiue, Lianqi Zhang, Mamoru Watanabe, and Takayoshi Sasaki*,†

Advanced Materials Laboratory, National Institute for Materials Science, 1-1 Namiki, Tsukuba, Ibaraki 305-0044, Japan, and CREST, Japan Science and Technology Agency (JST)

Received December 10, 2002. Revised Manuscript Received August 4, 2003

A new type of layered Li−Mn-oxide with heavy stacking faults has been synthesized via flocculation of delaminated MnO_2 nanosheets with Li ions. Flocculated products were characterized by powder X-ray diffraction, thermal analysis, scanning electron microscopy, transmission electron microscopy, chemical analysis, N_2 adsorption, and electrochemical measurements. Chemical analysis and X-ray diffraction results indicated that the colloidal MnO_2 nanosheets were restacked to produce a lamellar material $Li_{0.36}MnO_2 \cdot 1.15H_2O$ with a basal distance of 0.72 nm. Simulation of the X-ray diffraction profile suggested that the sheet-to-sheet registry was nearly random with partial order (20−40%) involving a shift vector of ($^1/_3$, $^2/_3$, 1). A disordered mesoporous texture was resulted via the stacking of a limited number of the sheets and irregular aggregation of the resulting restacked crystallites. The structure proved to be stable during low-temperature soft-chemical synthetic processes while thermo-metastable upon heat treatment. A dehydrated sample of this new layered Li−Mn-oxide underwent electrochemical Li^+ insertion/extraction behavior with smooth cycling curves.

Introduction

Nanoscale materials with low dimensionality have attracted much attention due to their novel physicochemical properties in comparison with bulk materials. Zero-dimensional nanoparticles and one-dimensional nanostructures, such as nanotubes, nanowires, and nanorods, have been intensively investigated.[1−4] Recently, a variety of unilamellar two-dimensional crystallites have been synthesized by chemically delaminating a layered host into molecular single layers.[5−7] The resulting elementary layers, so-called "nanosheets" or "inorganic two-dimensional macromolecules", have a number of interesting aspects with respect to highly two-dimensional anisotropy and ultrathin thickness in nano- or subnanometer scale, well-defined composition, and highly crystalline nature. By using these nanosheets as inorganic building blocks, novel nanostructured systems with well-tailored architectures, such as multilayer ultrathin films, hollow shells, and thin flakes, have been successfully fabricated.[8−10]

The restacking of nanosheets via flocculation provides an effective route to the fabrication of novel materials which are difficult to attain via conventional synthetic techniques.[11−13] The resulting products consisting of restacked nanosheets often exhibit a disordered layered

* Corresponding author. Fax: +81-29-854-9061. E-mail: sasaki.takayoshi@nims.go.jp.

† CREST, Japan Science and Technology Agency (JST).

(1) (a) Nelson, J. A.; Wagner, M. J. *Chem. Mater.* **2002**, *14*, 915. (b) O'Brien, S.; Brus, L.; Murray, C. B. *J. Am. Chem. Soc.* **2001**, *123*, 12085.

(2) (a) Iijima, S. *Nature* **1991**, *354*, 56. (b) Patzke, G. R.; Krumeich, F.; Nesper, R. *Angew. Chem., Int. Ed.* **2002**, *41*, 2446. (c) Kasuga, T.; Hiramatsu, M.; Hoson, A.; Sekino, T.; Niihara, K. *Langmuir* **1998**, *14*, 3160. (d) Wang, L. Z.; Tomura, S.; Ohashi, F.; Maeda, M.; Suzuki, M.; Inukai, K. *J. Mater. Chem.* **2001**, *11*, 1465. (e) Han, W.; Bando, Y.; Kurashima, K.; Sato, T. *Appl. Phys. Lett.* **1998**, *73*, 3085.

(3) (a) Duan, X. F.; Huang, Y.; Cui, Y.; Wang, J.-F.; Leiber, C. M. *Nature* **2001**, *409*, 66. (b) Hu, J.-T.; Odom, T. W.; Lieber, C. M. *Acc. Chem. Res.* **1999**, *32*, 435. (c) Zhang, D.; Qi, L.; Ma, J.; Cheng, H. *Chem. Mater.* **2001**, *13*, 2753. (d) Wang, L. Z.; Shi, J.-L.; Zhang, W.-H.; Ruan, M.-L.; Yu, J.; Yan, D.-S. *Chem. Mater.* **1999**, *11*, 3015.

(4) (a) Tian, Z.-R.; Voigt, J. A.; Liu, J.; Mckenzie, B.; Mcdermott, M. J. *J. Am. Chem. Soc.* **2002**, *124*, 12954. (b) Urban, J. J.; Yun, W.-S.; Gu, Q.; Park, H. *J. Am. Chem. Soc.* **2002**, *124*, 1186. (c) Yang, J.; Zeng, J.-H.; Yu, S.-H.; Yang, L.; Zhou, G.-E.; Qian, Y.-T. *Chem. Mater.* **2000**, *12*, 3259.

(5) (a) Kaschak, D. M.; Johnson, S. A.; Hooks, D. E.; Kim, H.-N.; Ward, M. D.; Mallouk, T. E. *J. Am. Chem. Soc.* **1998**, *120*, 10887. (b) Zhang, Z.; Lerner, M. M. *Chem. Mater.* **1996**, *8*, 257.

(6) (a) Wang, Z.; Pinnavaia, T. J. *Chem. Mater.* **1998**, *10*, 1820. (b) Han, Y.-S.; Park, I.; Choy, J.-H. *J. Mater. Chem.* **2001**, *11*, 1277. (c) Wang, L.; Kanatzidis, M. G. *Chem. Mater.* **2001**, *13*, 3717. (d). Liu Z.-H.; Ooi, K.; Kanoh, H.; Tang, W.-P.; Tomida, T. *Langmuir* **2000**, *16*, 4154.

(7) (a) Sasaki, T.; Watanabe, M.; Hashizume, H.; Yamada, H.; Nakazawa, H. *J. Am. Chem. Soc.* **1996**, *118*, 8329. (b) Sasaki, T.; Watanabe, M. *J. Am. Chem. Soc.* **1998**, *120*, 4682.

(8) (a) Kotov, N. A.; Dékány, I.; Fendler, J. H. *Adv. Mater.* **1996**, *8*, 637. (b) Cassagneau, T.; Fendler, J. H. *Adv. Mater.* **1998**, *10*, 877.

(9) (a) Schaak, R. E.; Mallouk, T. E. *Chem. Mater.* **2000**, *12*, 2513. (b) Schaak, R. E.; Mallouk, T. E. *Chem. Mater.* **2000**, *12*, 3427.

(10) (a) Sasaki, T.; Ebina, Y.; Watanabe, M.; Decher, G. *Chem. Commun.* **2000**, 2163. (b) Sasaki, T.; Ebina, Y.; Tanaka, T.; Harada, M.; Watanabe, M.; Decher, G. *Chem. Mater.* **2001**, *13*, 4661. (c) Sasaki, T.; Nakano, S.; Yamauchi, S.; Watanabe, M. *Chem. Mater.* **1997**, *9*, 602. (d) Iida, M.; Sasaki, T.; Watanabe, M. *Chem. Mater.* **1998**, *10*, 3780. (e) Wang, L. Z.; Sasaki, T.; Ebina, Y.; Kurashima, K.; Watanabe, M. *Chem. Mater.* **2002**, *14*, 4827. (f) Wang, L. Z.; Omomo, Y.; Sakai, N.; Fukuda, K.; Nakai, I.; Ebina, Y.; Takada, K.; Watanabe, M.; Sasaki, T. *Chem. Mater.* **2003**, *15*, 2873.

10.1021/cm0217809 CCC: $25.00
Published on Web 10/14/2003

structure involving irregular orientation and lateral displacement of the nanosheets. Some unique features, such as structural disorder, high surface area, and homogeneously dispersed guest species, can be readily introduced in the products, which often offers beneficial advantages for some applications, including catalysis and photocatalysis.[11]

Manganese oxides are of considerable interest due to their versatile range of catalytic, electrochemical, ion-exchange, and magnetic properties.[14−16] Recently, we have examined the synthesis, acid-exchange property, and exfoliation behavior of layered materials of A_xMnO_2, where A represents alkali metals such as K and Na.[17] Colloidal MnO_2 nanosheets have been successfully obtained by delaminating an acid-exchanged form of $K_{0.45}MnO_2$[18] with tetrabutylammonium (TBA^+) ions. The resulting nanosheet consists of a two-dimensional array of edge-shared MnO_6 octahedra with a crystallographic thickness of ca. 0.5 nm. In the present work, we studied the restacking of the colloidal MnO_2 nanosheets by flocculation with Li ions, the preparation procedure of which is schematically depicted in Scheme 1. This layered Li−Mn-oxide with a disordered arrangement of nanosheets exhibited smooth voltage profiles upon electrochemical discharge/charge cycling.

Scheme 1. Procedures for Fabricating Li−Mn-oxide with Disordered Layer Stacking

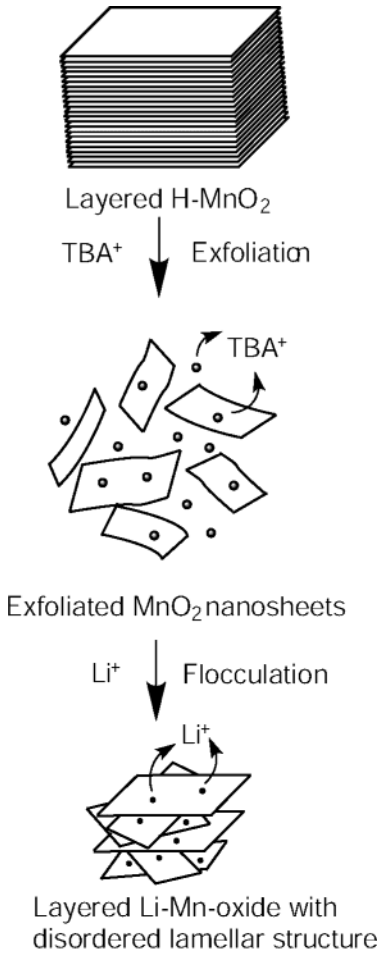

Experimental Section

Materials. K_2CO_3 (Wako Pure Chemical Co., Japan) and Mn_2O_3 (High Purity Chemical Co., Japan) were of 99.9% purity. All other chemicals were of analytical grade and were obtained from commercial sources. Ultrapure water (>17 MΩ cm) from a Milli-Q water system was used throughout the experiments.

Synthesis and Exfoliation of Layered $K_{0.45}MnO_2$. The starting layered material of $K_{0.45}MnO_2$ was synthesized by a conventional solid-state procedure. K_2CO_3 and Mn_2O_3 were mixed intimately and then heated at 750 °C for 30 h under an O_2 gas flow to produce $K_{0.45}MnO_2$. Its XRD data were consistent with that reported in the literature.[19] A protonic form of layered manganese oxide was prepared by digesting the layered $K_{0.45}MnO_2$ (∼10 g) with 2 dm^3 of a 1 mol dm^{-3} HCl aqueous solution at room temperature for 10 d. The HCl solution was refreshed every day to ensure the completeness of protonation. The resulting product of $H_{0.13}MnO_2{\cdot}0.7H_2O$ (H−MnO_2) was collected by filtration, washed with a copious amount of water, and then air-dried at ambient temperature. Colloidal suspensions of MnO_2 were prepared by mixing 0.4 g of H−MnO_2 with 100 cm^3 of tetrabutylammonium hydroxide ($(C_4H_9)_4NOH$) solution (5.2 mmol). The mixture was agitated vigorously at room temperature for 10 d. The unexfoliated component was then separated at 10 000 rpm using a magnetic centrifuge to obtain the suspension containing well-dispersed exfoliated manganese oxide nanosheets.

Restacking of Nanosheets. Restacking of the nanosheets was induced by mixing the colloidal suspension of MnO_2 nanosheets with a LiOH solution. In a typical experiment, 200 cm^3 of MnO_2 nanosheet suspension (0.8 g dm^{-3}) was dropped into 200 cm^3 of 1 mol dm^{-3} LiOH solution at a rate of ca. 1 cm^3/min. Immediately after the addition of nanosheet suspension, flocculation occurred in the mixed solution. The flocculated precipitate was recovered by filtration, washed with water, and air-dried at room temperature.

Electrochemical Measurements. The as-prepared restacked Li−Mn-oxide was evacuated at 150 °C to expel the water molecules from its interlayer galleries. The vacuum-dried sample was mixed with 20 wt % carbon black and 10 wt % poly(tetrafluoroethylene) (PTFE) to make cathodes for electrochemical measurements. The measurements were performed in a coin-type cell using 1 mol dm^{-3} $LiClO_4$ solution in mixed ethylene carbonate (EC) and diethyl carbonate (DEC) (1:1 in volume) as the electrolyte and metallic Li as the anode. The cell was discharged and charged at a constant current density of 44 μA cm^{-2} between 2.5 and 4.5 V at ambient temperature.

Characterization. X-ray diffraction (XRD) data were collected using a Rigaku Rint 2000 powder diffractometer with Cu Kα radiation (λ = 0.15405 nm). Scanning electron microscopy (SEM) observations on the restacked aggregates were

(11) (a) Ebina, Y.; Sasaki, T.; Harada, M.; Watanabe, M. *Chem. Mater.* **2002**, *14*, 4390. (b) Domen, K.; Ebina, Y.; Ikeda, S.; Tanaka, A.; Kondo, J. N.; Maruya, K. *Catal. Today*, **1996**, *28*, 167.

(12) (a) Liu, P.; Gong, K.; Xiao, P.; Xiao, M. *J. Mater. Chem.* **2000**, *10*, 933. (b) Sukpirom, N.; Lerner, M. M. *Chem. Mater.* **2001**, *13*, 2179. (c) Strawhecker, K. E.; Manias, E. *Chem. Mater.* **2000**, *12*, 2943.

(13) (a) Xu, Y.-H.; Feng, Q.; Kajiyoshi, K.; Yanagisawa, K.; Yang, X.-J.; Makita, S.; Ooi, K. *Chem. Mater.* **2002**, *14*, 3844. (b) Liu, Z.-H.; Yang, X.-J.; Makita, Y.; Ooi, K. *Chem. Lett.* **2002**, 680. (c) Liu, Z.-H.; Yang, X.-J.; Makita, Y.; Ooi, K. *Chem. Mater.* **2002**, *14*, 4800.

(14) (a) Shen Y.-F.; Zerger, R. P.; DeGuzman, R. N.; Suib. S. L.; McCurdy, L.; Potter, D. I.; O'Young, C. L. *Science* **1993**, 260, 511. (b) Tian, Z.-R.; Tong, W.; Wang, J.-Y.; Duan, N.-G.; Krishnan, V. V.; Suib, S. L. *Science* **1997**, *276*, 926. (c) Ma, Y.; Suib, S. L.; Ressler, T.; Wong, J.; Lovallo, M.; Tsapatsis, M. *Chem. Mater.* **1999**, *11*, 3545.

(15) (a) Feng, Q.; Kanoh, H.; Ooi, K. *J. Mater. Chem.* **1999**, *9*, 319. (b) Brock, S. L.; Sanabria, M.; Nair, J.; Suib, S. L.; Ressler, T. *J. Phys. Chem. B* **2001**, *105*, 5404.

(16) (a) Kim, J.; Manthiram, A. *Nature* **1997**, *390*, 265. (b) Armstrong, A. R.; Bruce, P. G. *Nature* **1996**, *381*, 499.

(17) (a) Omomo, Y.; Sasaki, T.; Watanabe, M. *Solid State Ionics* **2002**, *151*, 243. (b) Omomo, Y.; Sasaki, T.; Wang, L. Z.; Watanabe, M. *J. Am. Chem. Soc.* **2003**, *125*, 3568.

(18) The acid-exchanged phase of $K_{0.45}MnO_2$ was in higher crystallinity and was exfoliated more easily in comparison with a protonic oxide from $NaMnO_2$.

(19) Delmas, C.; Fouassier, C. *Z. Anorg. Allg. Chem.* **1976**, *420*, 184.

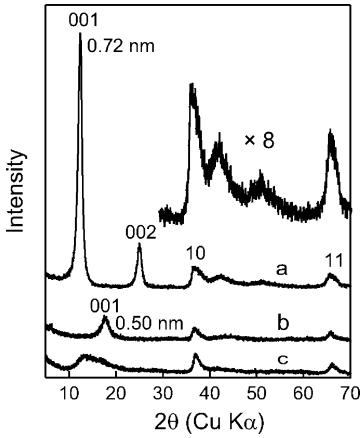

Figure 1. XRD patterns of restacked Li−Mn-oxide: (a) as-synthesized; (b) dried under vacuum at 150 °C; (c) rehydrated by exposing the dehydrated sample in moisture at ambient temperature.

conducted with a JEOL JSM-5800LV instrument operated at 15 kV. Samples were sputter-coated with a thin layer of Au (ca. 10 nm). TEM observations and selected-area electron diffraction measurements were performed using a JEOL 1010 transmission electron microscope operated at 100 kV. Specimens were prepared by placing a drop of ethanol suspension of the dispersed Li−Mn-oxide onto a copper grid. Thermogravimetric analysis (TGA) data were acquired under airflow using a Rigaku TG-8120 instrument at a heating rate of 10 °C/min. The N_2 adsorption−desorption isotherms were determined using a BELSORP 28SA equipment. The sample was dried by evacuation at 150 °C prior to measurements. The specific surface area (S_{BET}) was calculated from the linear part of the BET plot ($P/P_0 = 0.10-0.30$) and the pore size distribution was calculated employing the Dollimore−Heal (DH) method from the adsorption branch of N_2 isotherms. The elemental compositions were determined by an IRIS inductively coupled plasma (ICP) spectrometer (Nippon Jarrell-ash Co., Ltd) after dissolving a weighed amount of sample in a mixed solution of HNO_3 and H_2O_2. The C and H_2O contents were obtained using LECO carbon and water analyzers. The average oxidation state of Mn was determined by dissolution of the Li−Mn-oxide in a mixed solution of $(COONa)_2$ and H_2SO_4 at elevated temperature and subsequent titration of the excess $(COONa)_2$ using $KMnO_4$.[20]

Results and Discussion

Characterizations of Restacked Nanosheets. The composition of the flocculated product was determined to be $Li_{0.36}MnO_2 \cdot 1.15H_2O$ by chemical analysis (Calcd: Li, 2.3%; Mn, 49.9%, H_2O, 18.8%. Found: Li, 2.3%; Mn, 50.1%; H_2O, 18.8%). The chemical titration results revealed that the average oxidation state for Mn in the restacked Li−Mn-oxide was 3.85, being close to that for its starting protonic H−MnO_2 (3.86). Its X-ray diffraction pattern was distinct from those of materials with three-dimensional crystalline order (see Figure 1a). The two pronounced diffraction peaks at 12.3° (2θ) and 25.1° (2θ) can be indexed as 001 and 002 of basal series, indicating a lamellar structure with a basal spacing of 0.72 nm. On the other hand, the broad peaks around 36.5° and 65.6° in 2θ are indexable as intrasheet reflections of 10 and 11 for the two-dimensional hexagonal cell with $a = 0.284$ nm, respectively. These diffraction bands indicated that the hexagonal atomic arrangement of the nanosheets was preserved after the flocculation. One of the most important features here is the absence of general *hkl* reflections and the asymmetric profile of the 10 and 11 bands with a tail toward a higher angular side. This is characteristic of a disordered lamellar structure, indicating that the nanosheets were restacked without regular sheet-stacking sequence.[10c]

SEM image (Figure 2a) revealed that the sample was composed of large agglomerations of loosely and irregularly piled-up platy particles in the range of 5−40 μm, which is consistent with the synthetic procedure in this study. TEM observations also confirmed the aggregated morphology of the samples (Figure 2b). Some thin platelets, which may consist of a few pieces of restacked nanosheets, could also be distinguished from the edge regions of the aggregates, supporting the restacking of the nanosheets. The selected-area electron

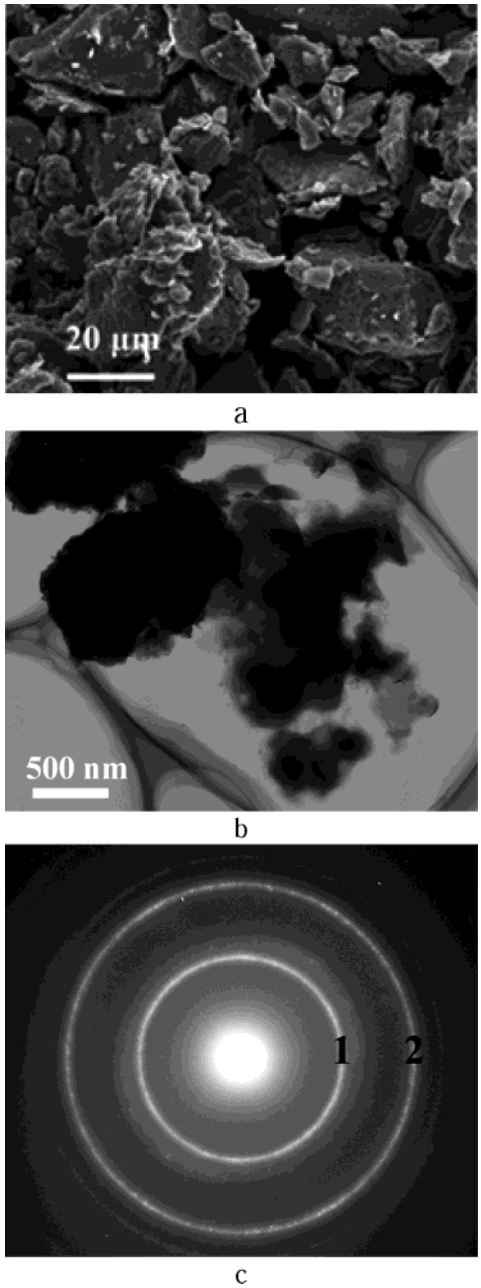

Figure 2. SEM (a) and TEM (b) images and electron diffraction pattern (c) of the restacked Li−Mn-oxide.

(20) JIS M 8233. Methods for determination of active oxygen in manganese ores; Japanese Industrial Standards Committee, 1969.

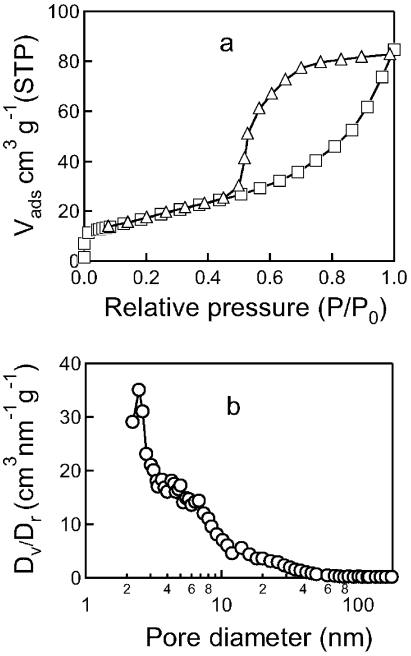

Figure 3. Nitrogen adsorption (square markers)−desorption (triangular markers) isotherms (a) of the restacked Li−Mn-oxide, and its pore-size distribution derived from adsorption branch (b).

diffraction pattern (Figure 2c) of the sample gave a series of concentric diffraction rings, which are attributable to the two-dimensional hexagonal lattice of the nanosheets.[21] The indices and spacings for diffraction rings 1 and 2 were (1) 10, 0.246 nm and (2) 11, 0.145 nm, respectively, being consistent with the XRD data.

The material had a relatively high specific surface area of 65 $m^2\ g^{-1}$ as determined by the multi-point BET method. This was significantly higher than that of its parent material $K_{0.45}MnO_2$ with ca. 2 $m^2\ g^{-1}$. The N_2 adsorption−desorption isotherms (Figure 3a) can be classified as type IV with a noticeable H3 hysteresis loop, which is characteristic of slitlike pores. Analysis of the adsorption isotherm branch revealed the broad distribution of mesopores in the diameter range of 2−10 nm for the material (Figure 3b). The openings and voids between the lamellar crystallites composed of stacked two-dimensional nanosheets may be attributable to this disordered porous structure. Similar porous features have been observed in restacked layered materials.[10c,22] This nanoporous nature may be particularly suitable for use as a cathode material because electrolytes can readily access and fill the inner-surface of the material to give a large electrode area.

Figure 4 depicts the TGA data for the Li−Mn-oxide material. The sample lost weight of approximately 16.5% between ambient temperature and 200 °C, accompanied by two endothermic peaks. These thermal events are attributable to evaporation of the intersheet water. Further weight loss was observed at higher temperature, which may be ascribed to the formation of new phases involving the oxygen release. The structural evolution of the material upon heat treatment was examined by XRD (Figure 5). The original structure remained unchanged after being treated at 100 °C for 1 h, whereas the 001 peak became weak after heat treatment at 200 °C in air, corresponding to the removal of water from the material. A new XRD peak with a *d* value of ca. 0.48 nm appeared above 300 °C. This peak enhanced progressively and additional new peaks appeared at higher heating temperature, which are identifiable as spinel $LiMn_2O_4$ as a major phase and a small proportion of Mn_2O_3.

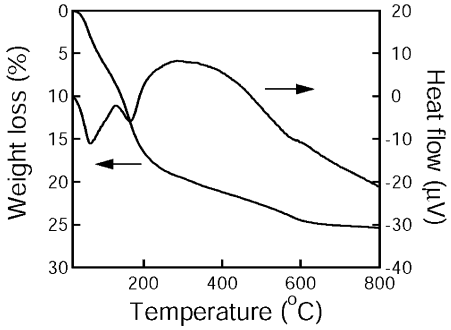

Figure 4. TG and DTA curves of the restacked Li−Mn-oxide.

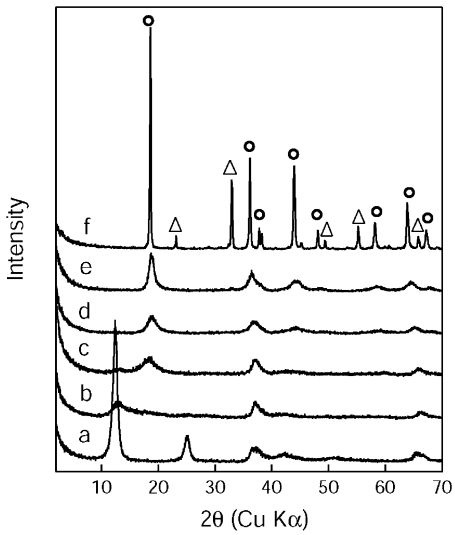

Figure 5. XRD patterns for the restacked Li−Mn-oxide heated at different temperatures. (a) 100 °C × 1 h; (b) 200 °C × 1 h; (c) 300 °C × 1 h; (d) 400 °C × 1 h; (e) 500 °C × 1 h; (f) 800 °C × 1 h. Inserted symbols ○ and △ represent $LiMn_2O_4$ and Mn_2O_3, respectively.

XRD Profile Simulation. To obtain insight into structural aspects of the flocculated material, we carried out the simulation of X-ray diffraction patterns for a disordered layered system. The analysis on diffuse scattering intensities, *I*, from a disordered structure involving stacking faults has been formulated as[23]

$$I = \sum_{m=-(N-1)}^{N-1} (N - |m|)\left\{\sum_{s=1}^{r}\sum_{t=1}^{r} p_{st}^{(m)} F_s F_t^*\right\} \exp(2\pi i \mathbf{s}\cdot\mathbf{R})$$

where *N* is the number of fundamental sheets, **s** is a scattering vector, *F* is a sheet structure factor, and **R** is a displacement vector for a pair of *s*-th and *t*-th sheet. Only one kind of fundamental sheet is considered in the

(21) (a) Sasaki, T.; Watanabe, M. *J. Phys. Chem. B* **1997**, *101*, 10159. (b) Sasaki, T.; Ebina, Y.; Kitami, Y.; Watanabe, M.; Oikawa, T. *J. Phys. Chem. B* **2001**, *105*, 6116.

(22) (a) Choy, J.-H.; Lee, H.-C.; Jung, H.; Kim, H.; Boo, H. *Chem. Mater.* **2002**, *14*, 2486. (b) Carrado, K. A.; Xu, L. *Microporous Mesoporous Mater.* **1999**, *27*, 87.

(23) Wilson, A. J. C. *Proc. R. Soc.* **1942**, *A180*, 277.

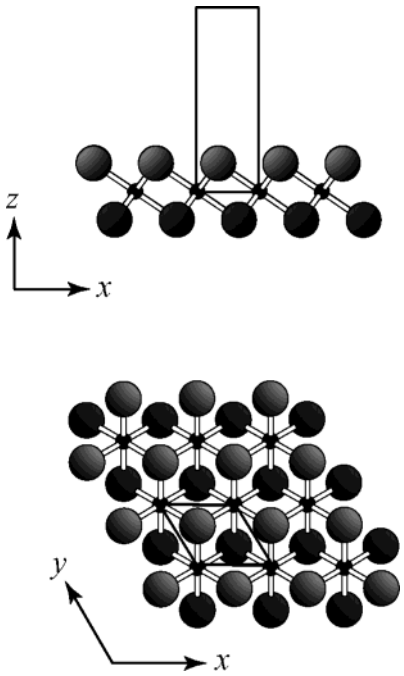

Figure 6. Structural model for a fundamental sheet of MnO_2. Smaller and larger circles denote Mn and O atoms, respectively. For the latter, darker and brighter ones are at z = −0.166 and 0.166, respectively. The solid lines encircle the unit cell.

Table 1. Structural Parameters for the Fundamental Sheet of MnO_2[a]

atom	*x*	*y*	*z*
Mn	0	0	0
O1	$^1/_3$	$^2/_3$	0.166[b]
O2	$^2/_3$	$^1/_3$	−0.166[b]

[a] Unit cell parameters: $a = 0.284$ nm, $c = 0.72$ nm. [b] Estimated based on the sheet thickness for birnessite.[27]

present case and its structure factor is calculated on the basis of a structure model shown in Figure 6 and Table 1. Stack operations are defined by placing a new fundamental sheet over the last stacked sheet after shifting the former by a specified vector (x, y, z). The suffix *r* is the number of shift vectors employed. The probability of $p_{st}^{(m)}$ is a probability for occurring *s*-th and *t*-th sheets with constant *m*, and is deduced from such probabilities for neighboring sheet pair related to a specified shift vector. The matrix method was applied to calculate the diffuse scattering profiles[24] using a program FU1.[25]

In the first step, we tried to reproduce a profile from completely disordered or the so-called turbostratic system by employing 6, 9, and 12 shift vectors, listed in Table 2. The shift along *x* and *y* were selected in a randomized way while the shift along *z* was set to 1, reflecting a constant intersheet separation of 0.72 nm in the present case. Probabilities for the shift vectors are assumed to be equal to represent random stacking of the sheets. The total number of sheets was set to 10, and profile parameters of Lorentz function representing

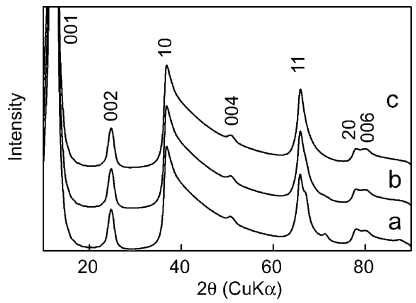

Figure 7. Simulated profiles for a completely disordered layered system. Traces a−c are obtained using 6, 9, and 12 shift vectors in Table 2 (from the top). $N = 10$.

Table 2. Shift Vectors Used in Simulation

shift vector	(*x*, *y*, *z*)
1	(0, 0, 1)
2	($^2/_3$, $^1/_3$, 1)
3	($^1/_3$, $^2/_3$, 1)
4	($^1/_2$, 0, 1)
5	($^1/_6$, $^1/_3$, 1)
6	($^5/_6$, $^2/_3$, 1)
7	(0, $^1/_2$, 1)
8	($^2/_3$, $^5/_6$, 1)
9	($^1/_3$, $^1/_6$, 1)
10	($^1/_2$, $^1/_2$, 1)
11	($^1/_6$, $^5/_6$, 1)
12	($^5/_6$, $^1/_6$, 1)

broad profiles were selected. These were selected by taking into account the fact that the number of the nanosheets restacked to form a crystallite was likely limited. As shown in Figure 7, *hk* diffraction bands arising from intrasheet periodicity evolved besides the basal lines. Traces calculated using 9 and 12 shift vectors showed smooth decay in a higher angular side of the diffraction bands,[26] being diagnostic of a profile from completely disordered stacking. In contrast, the data based on 6 shift vectors did not have a smooth profile particularly on a tail of 11 band, suggesting that 6 sets of shift vectors are not enough. On the basis of these results, we employed 12 shift vectors in further analysis.

The experimental profile for *hk* diffraction bands was similar to trace c in Figure 7 calculated on the basis of 12 shift vectors having equal probability (= $^1/_{12}$) for occurrence in that the bands exhibited an asymmetric tail toward a higher-angle side. However, there was a noticeable difference. The tail did not show a monotonic decay but had some wavy profile, which was relatively clear for the 10 band. The top of the broad humps was at 42.3° and 50.5° in 2θ, which correspond to positions of 105 and 108 peaks when we assume a hexagonal unit cell with lattice parameters $a = 0.284$ nm, $c = 3 \times 0.72$ nm. The tendency for the enhancement of *h*0*l* peak with $h + l = 3n$ may lead to a stacking model in which a probability for a shift vector ($^1/_3$, $^2/_3$, 1) prevails over those for the other sheet sequences. We calculated the profile on this assumption and the results are depicted in Figure 8. The bottom trace corresponds to that in Figure 7c, representing random stacking. On the other hand, the top pattern represents the profile in full order where all the sheets are stacked in a sequence regulated

(24) (a) Hendricks, S.; Teller, E. *J. Chem. Phys.* **1942**, *10*, 147. (b) Kakinoki, J.; Komura, Y. *Acta Crystallogr.* **1965**, *19*, 137. (c) Kakinoki, J. *Acta Crystallogr.* **1967**, *23*, 875. (d) Onoda, M.; Kawada, I. *Acta Crystallogr. Sect. A* **1980**, *36*, 134. (e) Onoda, M.; Chen, X.-A.; Sato, A.; Wada, H. *J. Solid State Chem.* **2000**, *152*, 332.

(25) Kato, K. FU1, personal communication, 1991.

(26) Note that small peaks (50° and 80° in 2θ) in the tail of 10 and 20 bands are attributable to basal reflections.

(27) Post, J. E.; Veblen, D. R. *Am. Mineral.* **1990**, *75*, 477.

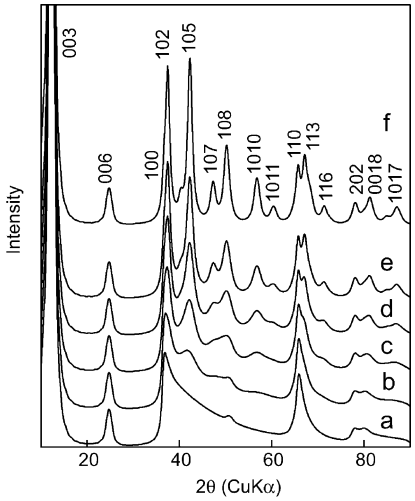

Figure 8. Simulated profiles assuming various degrees of order. Trace (a) is based on the random appearance of 12 shift vectors, whereas (b)−(f) are calculated assuming probabilities of 20, 40, 60, 80, and 100%, respectively, for the shift vector 3 in Table 2 (probabilities for the others are all equal). $N = 10$.

by the shift vector ($^1/_3$, $^2/_3$, 1). This layer sequence leads to a rhombohedral lattice in $R3m$ symmetry. The indices are given in Figure 8f. Among a series of profiles calculated on the basis of intermediate degrees of order, the traces calculated with a probability of 20−40% for the shift vector ($^1/_3$, $^2/_3$, 1) showed close similarity to the experimental data. On the basis of these calculated results, it may be concluded that the flocculated material had a disordered structure in which the layer sequence involving the shift vector ($^1/_3$, $^2/_3$, 1) had a probability of 20−40% and the other stacking modes were random. The stacking with the shift mode of ($^1/_3$, $^2/_3$, 1) produces trigonal prismatic sites in the intersheet gallery, which are suitable in accommodating guest species with a size comparable to that of a water molecule. This may rationalize higher probability for occurrence of the shift vector ($^1/_3$, $^2/_3$, 1) than for the others.

Electrochemical Measurements. For the purpose of electrochemical measurements, the material should be free from water. To remove the interlayer water, the sample was dried at 150 °C under vacuum for 4 h. The XRD measurements for the resulting dehydrated material were performed using a specially designed sample holder filled with argon gas to prevent moisture uptake. The material maintained the disordered structure, although the basal spacing diminished to ca. 0.50 nm (see Figure 1b). Intensity was considerably reduced, but asymmetric hk diffraction bands were discernible. The dehydrated sample exhibited reswelling behavior by exposing the material in moisture, as shown in Figure 1c, suggesting that the layer structure remained practically unchanged after vacuum-drying at this temperature. The basal spacing of the material expanded to ca. 0.65 nm again after the dehydrated sample was exposed to moisture or immersed in water and dried again at ambient temperature, which is attributable to the reinsertion of water molecules into galleries of restacked sheets. Accordingly, the apparently different basal spacing observed for the dehydrated material at 200 °C in air may be reasonably elucidated by this rehydration behavior of the material because the data in Figure 5 were measured in air.

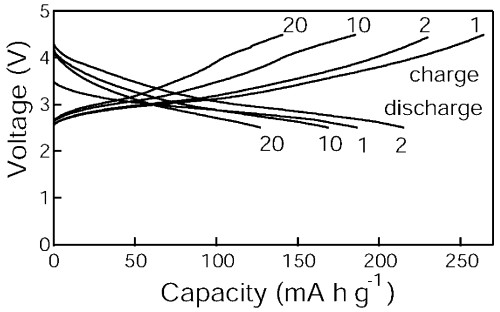

Figure 9. Discharge−charge curves of the restacked Li−Mn-oxide. Current density: 44 μA cm^{-2}.

The vacuum-dried sample was mixed with carbon black and PTFE to make cathodes for electrochemical measurements. A capacity of 190 mA h g^{-1} was obtained in the first discharge process (Figure 9). This corresponds to insertion of ca. 0.64 Li units per Mn in the formula, indicating that most Mn ions in the material were reduced to trivalent state accompanied by Li^+ insertion to $LiMnO_2$. The following charge process exhibited a very high capacity of 266 mA h g^{-1}, suggesting the extraction of about 93% (theoretical capacity) of lithium. The charge and discharge capacities tended to decrease upon cycling, as was shown in Figure 9. A complete understanding in the capacity fading is not yet available. The formation of some electrochemical inactive phases or dissolution of the material may be a possible explanation. Further studies on the electrochemical performance of this material are now in progress.

Although the capacity decreased continuously, relatively smooth discharge−charge curves with nearly constant slopes were observed over the whole range of Li insertion/extraction processes. The disordered nature of the Li−Mn-oxide may be responsible for this behavior because Li ions are expected to have a range of coordination environments in the material. From a practical point of view, this feature is advantageous in overcoming the problem associated with over discharge−charge.[16a]

Over the past several years, demand for rechargeable lithium batteries as power sources in portable electronic devices has been growing very rapidly.[28] Layered $LiMnO_2$ in rhombohedral symmetry, which can offer a theoretical charging/discharging capacity of ca. 286 mA h g^{-1}, is an attractive alternative to the $LiCoO_2$ currently used in lithium batteries with respect to cost, toxicity, and safety.[16b] However, the layered $LiMnO_2$ is not structurally stable during electrochemical insertion/extraction of Li and is easily converted to the more stable spinel structure. This instability is attributable to the structural similarity in layered $LiMnO_2$ and spinel. In both materials, the oxygen atom planes are stacked in cubic close-packed fashion (ABC sequence) and the structures differ only by minor cationic arrangement. Consequently, conversion of the layered structure to the more stable spinel during electrochemical insertion/extraction of Li ions can easily take place.

In the present material, after 20 discharge/charge cycles, only a very small plateau was discernible at ca. 4.0 V but no apparent one was discernible at 3.0 V,

(28) Tarascon, M.; Armand, M. *Nature* **2001**, *414*, 359.

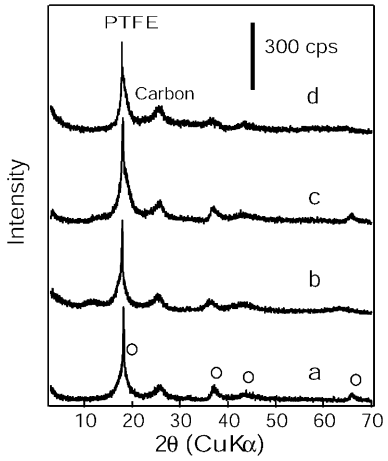

Figure 10. XRD patterns of cathodes at various stages of electrochemical measurement: (a) starting Li−Mn-oxide mixed with carbon black and PTFE with weight ratio of 7:2:1; (b) after first discharge process; (c) after first discharge/charge cycle; (d) after 20 discharge/charge cycles. Inserted symbol ○ represents the peaks for Li−Mn-oxide.

which are characteristic of spinel phase. This relatively smooth charge/discharge slopes without well-defined plateaus were apparently different from that for known layered $LiMnO_2$. The layered $LiMnO_2$ reported so far generally undergoes phase transformation into spinel in the first several cycles accompanied by evolution of a clear voltage profile feature of spinel structure with 3 V and 4 V plateaus.[29,30] The disordered lamellar structure in Li−Mn-oxide is expected to play a role in inhibiting the rapid phase transformation because the irregular layer-to-layer registry may provide a high energy barrier against the phase conversion toward the spinel structure. XRD data after discharge−charge cycles also confirmed this, showing no apparent structural change in the cathode after 20 cycles (see Figure 10) except for appearance of a shoulder around 2θ of 18.5°. Note that a sharp XRD peak representing the PTFE binder was located at the 2θ position similar to that of layered Li−Mn-oxide, resulting in an overlapped profile centered at ca. 18.0° (2θ). It is difficult to identify the shoulder peak at the present stage, but the peak may be attributable to a limited amount of spinel phase that may explain the slight plateaulike feature at 4.0 V in the charge process. It should be emphasized that the total phase transformation did not take place in the present material and only a limited amount of spinel phase, if any, was present after 10−20 cycles.

In summary, a new layered Li−Mn-oxide has been synthesized via flocculation of MnO_2 nanosheets. Structural characterizations revealed the disordered and porous nature of the material. Electrochemical data showed its smooth charge/discharge feature as a cathode material.

CM0217809

(29) Ammundsen, B.; Paulsen, J. *Adv. Mater.* **2001**, *13*, 943.
(30) Choi, S. Manthiran, A. *J. Electrochem. Soc.* **2002**, *149*, A1157.